ArF Laser-Induced Chemical Vapor Deposition of Polythiene Films from Carbon Disulfide

Radmila Tomovska,[†] Zdeněk Bastl,[‡] Vladimír Vorlíček,[§] Karel Vacek,[†] Jan Šubrt,[||] Zbyněk Plzák,[||] and Josef Pola*,[†]

Laser Chemistry Group, Institute of Chemical Process Fundamentals, Academy of Sciences of the Czech Republic, 16502 Prague, Czech Republic, J. Heyrovský Institute of Physical Chemistry, Academy of Sciences of the Czech Republic, 18223 Prague, Czech Republic, Institute of Physics, Academy of Sciences of the Czech Republic, 18040 Prague, Czech Republic, and Institute of Inorganic Chemistry, Academy of Sciences of the Czech Republic, 25068 Řež near Prague, Czech Republic

Received: February 18, 2003; In Final Form: June 23, 2003

Laser photolysis at 193 nm of gaseous carbon disulfide into CS and S in the absence and excess of N_2 is controlled by two-photon-induced depletion of CS_2 and affords chemical vapor deposition of $(CS)_n$ polymer and S_n. The proposed polymerization mechanism of CS is explained by an intermediacy of C_2S_2 species. The $(CS)_n$ polymer contains S-centered radicals that are stable in air and withstand heating in a H_2 atmosphere. Its structure is contributed by >C═S, >C═C<, S_2C═CS_2, −C−(C═S)−S−, −S−(C═S)−S−, and C−S−S−C configurations whose relative extent depends on irradiation conditions: more C═S bonds (and fewer C−S bonds) are formed at higher CS_2 pressure, in the excess of N_2 and with lower laser fluences. The extent of the S_2C═CS_2 units decreases, and that of >C═C< units increases, upon mild polymer heating. The polymer deposited in the absence of N_2 consists of unique 100−200 nm sized hollow spheres.

1. Introduction

Interaction of carbon disulfide with UV/vis radiation producing C/S polymeric substances was first examined more than a century ago.[1,2] The UV spectrum of CS_2 consists of a moderately intense absorption band between 280 and 390 nm and a much more intense band at 230−190 nm[3].

The irradiations resonant with the 280−390 nm band are regarded to induce[4−20] photopolymerization of CS_2 molecules through mechanisms similar in the gas and liquid phase. Thus, the gas-phase photolysis was interpreted to take place via primary excitation of CS_2 molecules (into CS_2*) and via either $CS_2 + CS_2^* \rightarrow 2CS + S_2$ (refs 4, 5, and 7), or $CS_2 + CS_2^* \rightarrow (CS_2)_2^* \rightarrow CS_3 + CS$, $2CS_3 \rightarrow 2CS_2 + S_2$, ref 12) steps. The liquid-phase photolysis was inferred[20] to occur via coupling and polymerizing of CS_2 molecules followed (to some extent) by elimination of S_2, which yielded a polymerizing S_2C_2 intermediate.

A single and a multiple photon absorption in CS_2 using high-energy photons of ArF, KrF, and YAG lasers initiate[21−27] photolytic dissociation of CS_2 molecules into S atoms and carbon sulfide (CS) and provides, in principle, conditions for a polymerization/copolymerization of S atoms, CS, and CS_2 molecules.

The mechanism of both long-[5−8,12,17,18] and short-wavelength[21−27] photolyses was examined, but the solid polymeric materials have been characterized[10,11,14,15,19,20] only for the former process.

Physical properties of the C/S polymeric materials produced by the long-wavelength photolysis of gaseous CS_2 were found as nearly identical to Bridgman's carbon disulfide prepared[28] from CS_2 at high pressures and temperature. The gas-phase-deposited material was described as $(CS_2)_x$ polymer,[7,15] a blend[10] of C polymer and S polymer, or $(CS)_x$ polymer,[5] whereas the liquid-phase-deposited material was ascertained as a mixture of conjugated $(CS_2)_x$ and $(C_3S_2)_x$ (ref 14) and a blend of $(CS_2)_x$ and $(CS)_x$ polymers cross-linked through disulfide linkages.[20]

However, and surprisingly, the polymeric products produced through primary photodissociation of CS_2 into CS and S fragments remain entirely unexplored. It was only concluded that the CS photolytically generated in the gas phase produced a brown solid deposit through wall reactions[29] and that the loss of the gas-phase (low-pressure-microwave discharge-generated) CS is not accompanied by the formation of a solid $(CS)_n$ polymer but is controlled by heterogeneous wall reaction giving CS_2 and carbonaceous polymer.[30]

Polymerization of carbon sulfide (CS) should in principle represent a feasible way to a highly conjugated $(CS)_n$ polymer that is of high interest due to appealing properties (magnetic effects, dopability) of conjugated sulfur-containing polymers (e.g., refs 31−33). A hypothetical $(CS)_n$ polymer that conceptually derives from the experimentally known trithiapentalene (described by structures I and II) has been proposed[34] but not yet obtained.

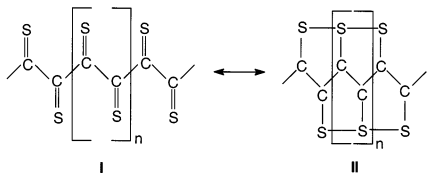

I II

Encouraged by the possibility of different reaction paths of CS transients in different conditions, we continued our earlier studies on laser photolytic chemical deposition of novel polymers (e.g., refs 35−38) and examined final reaction products formed from CS generated by ArF laser-induced gas-phase photolysis of CS_2. We report that the photolytically generated

[†] Laser Chemistry Group.
[‡] J. Heyrovský Institute of Physical Chemistry.
[§] Institute of Physics.
[||] Institute of Inorganic Chemistry.

10.1021/jp034411o CCC: $25.00
Published on Web 08/19/2003

CS undergoes gas-phase polymerization and yields $(CS)_n$ polymer whose structure consists of several different bonding arrangements between C and S atoms. We also show that the polymer structure depends on the photolytic conditions and that the polymer depositing from the gas phase in the absence of N_2 consists of unique hollow nanosized spheres that may find applications in nanoscience.

2. Experimental Section

Laser photolysis experiments were conducted on gaseous samples of CS_2 (10−100 Torr) without or at atmospheric pressure of nitrogen (total pressure 760 Torr) using an ArF (ELI 94 model) laser operating at 193 nm with a repetition frequency of 10 Hz. The samples were irradiated in a Pyrex reactor consisting of two orthogonally positioned tubes (both 3 cm in diameter), one (13 cm in length) furnished with KBr windows and the other (9 cm in length) equipped with quartz windows. The reactor had two sidearms, one fitted with a rubber septum and the other connecting to a vacuum line. It accommodated metal (Al, Cu), KBr, and quartz substrates, which, covered with the deposited solid material in the course of photolysis, were transferred for measurements of their properties by FTIR, UV, and X-ray photoelectron spectroscopy and electron microscopy. The metal substrates were washed prior to use by acetone in an ultrasonic bath. A laser beam at a pulse energy of 28−120 mJ, effective on an area of 2.3 cm^2, was used.

The progress of the CS_2 photolysis was monitored directly in the reactor by infrared spectroscopy (an FTIR spectrometer Nicolet Impact 400) using diagnostic bands at 1530 and 2180 cm^{-1}.

Laser photolysis of CS_2 (50 Torr)−ethene (100 Torr) mixtures without and in an excess of N_2 (total pressure 760 Torr) was carried out using a pulse energy of 45−114 mJ incident on an area of 2.3 cm^2. The photolysis products were examined directly in the reactor by FTIR spectrometry and also by gas chromatography−mass spectrometry (a QP 1000 Shimadzu mass spectrometer, Porapak P column, programmed (20−150 °C) temperature, He carrier gas).

Elemental analysis of the deposited films scrubbed from the substrate has been performed on a Perkin-Elmer 2400 analyzer; the results were reproducible within 10%.

The FTIR and UV spectra (a Shimadzu UV/vis 1601 spectrometer) of the deposited solid films were recorded after prolonged evacuation of the reactor.

Solid-state MAS (Magic Angle Spinning) NMR spectra were obtained on a Bruker DSX200 NMR spectrometer in a 5 mm broadband probe. ^{13}C were externally referenced to the carbonyl line of glycine ($\delta = 176.03$).

Raman spectra were recorded on a Renishaw (a Ramascope model 1000) Raman microscope coupled with a CCD detector. The exciting beam of an Ar-ion laser was defocused to obtain an energy density lower than 4×10^3 W/cm^2 and to diminish the heating of the sample.

EPR spectra were registered on a continuous wave (cw) X band spectrometer at room temperature at 1 mW microwave level and with 100 kHz modulation of 0.115 mT. The EPR spectra were taken before and after heating the solid powder in a closed ampule for 1 h to 250 °C in atmosphere of H_2 (130 kPa). An EPR simulation program Sim Fonia (Bruker, version 1.2) was used.

SEM photographs were obtained using a Philips XL30 CP Scanning electron microscope. TEM photomicrographs on samples scrubbed from the reactor surface and held with a copper grid were obtained using a Philips 201 transmission electron microscope.

X-ray photoelectron spectra (XPS) were measured with a Gammadata Scienta ESCA 310 electron spectrometer using monochromatized Al Kα ($h\nu = 1486.6$ eV) radiation for electron excitation. The high-resolution spectra of C 1s, O 1s, and S 2p photoelectrons were measured. Curve fitting of high-resolution spectra was accomplished using the lines of Gaussian−Lorentzian shape. For binding energy data we estimated the error limit ±0.2 eV. Photoelectron peak areas were calculated after removal of the Shirley background. The quantification of the superficial elemental concentrations was carried out by correcting the peak areas for the pertinent photoionization cross-sections and electron analyzer transmission function and by accounting for the dependence of the electron inelastic mean free paths on the kinetic energy.

Mass spectral analysis of the samples was performed on a MAGNUM GC−MS ion trap system (Finnigan MAT) equipped with heated inlet option (Spectronex AG, Basel, Switzerland)] and temperature programmed from 35 to 280 °C.

Thermogravimetric analysis of the solid deposit (sample weight 40 mg) was carried out by heating the sample up to 800 °C at the rate of 4 °C/min, using Cahn D-200 recording microbalances in a stream of argon. The sample sublimed upon heating was analyzed in a KBr pellet by FTIR spectroscopy.

Carbon disulfide was purchased from Aldrich (99.9% purity) and was distilled prior to use.

3. Results and Discussion

ArF laser photolysis of gaseous CS_2 and CS_2-N_2 results in depletion of CS_2 (no formation of volatile products) and fast formation of a brown fog. This phenomenon has been previously described[26] as the "laser snow effect".

The deposition has different features when carried out with or without N_2.

In the experiments without N_2, the fog formation could be seen with the naked eye in 30 s from the beginning of the irradiation. After several minutes of irradiation, the walls of the reactor were covered with a solid, showing different colors in different regions. The thin golden and tenaciously adherent solid films surviving the tape test were observed on the top walls, whereas dark and light brown thicker and nondhesive solid layers were accommodated on the reactor bottom and lower parts of the reactor. The distinctive formation of different color regions was particularly observed in the experiments with high incident fluence (>3.62 J cm^{-2}) and high CS_2 pressure (above 50 Torr). Moderately dissimilar IR spectra of these regions (see later) reflect their different structures.

In the experiments in excess of N_2, the fog formation was delayed by several tens of seconds and its deposition occurred only on the bottom of the reactor. The deposited solid was uniform by color (light brown), robust, and not adhesive at all and had static electricity.

3.1. Properties of Deposited Solids. The elemental analysis of the deposited materials obtained under similar irradiation conditions without and in excess of N_2 revealed the S to C ratios (S/C) to be close to 2. The analyses of both samples obtained in the absence and excess of N_2 done after washing the deposits with chloroform and CS_2 show that the C/S value changes dramatically and is equal to ∼1. The soluble fractions represent elemental sulfur and do not contain any polymer fraction, because their FTIR spectra show only a band at 471 cm^{-1} (S_8; see later). This finding and both C/S ratios being close to 1 reveal that the deposited material is composed of completely

TABLE 1: FTIR Spectra of Deposited Solids Obtained under Different Irradiation Conditions

deposit A	deposit B	deposit C		deposit D			deposit E	deposit F	deposit G
light brown	light brown	light brown	dark brown	light brown	dark brown	golden	dark brown	dark brown	light brown
Absorbance (cm^{-1}) (Relative Intensity[a])									
1780 (0.28)	1715 (0.95)	1701 (sh)	1693 (sh)	1705 (0.65)	1697 (0.84)	1690 (0.82)	1693 (0.77)	1699 (0.45)	1693 (5.20)
1703 (0.74)	1654 (sh)	1680 (0.76)	1674 (2.17)	1679 (sh)	1656 (sh)	1649 (sh)	1644 (sh)	1506 (4.00)	1633 (sh)
1654 (sh)	1509 (1.05)	1654 (sh)	1508 (6.30)	1507 (0.68)	1505 (3.18)	1508 (1.92)	1506 (4.16)	1454 (1.00)	1503 (1.90)
1506 (2.23)	1463 (1.00)	1504 (2.89)	1438 (1.00)	1455 (1.00)	1457 (1.00)	1454 (1.00)	1455 (1.00)	1363 (sh)	1470 (1.00)
1445 (1.00)	1403 (sh)	1456 (1.00)	1416 (sh)	1441 (sh)	1367 (sh)	1339 (0.16)	1390 (sh)	1288 (sh)	1439 (sh)
1369 (sh)	1370 (sh)	1430 (sh)	1352 (sh)	1360 (0.41)	1252 (0.09)	1252 (sh)	1370 (sh)	1255 (0.13)	1398 (sh)
1294 (sh)	1273 (0.44)	1402 (sh)	1215 (0.15)	1398 (sh)	1156 (0.29)	1224 (sh)	1257 (0.05)	1218 (sh)	1235 (0.15)
1257 (0.43)	1132 (0.79)	1216 (0.22)	1161 (0.98)	1224 (0.55)	1070 (0.36)	1202 (0.51)	1155 (0.29)	1153 (0.32)	1152 (0.76)
1227 (sh)	1081 (1.03)	1154 (0.49)	1074 (0.72)	1155 (0.89)	1003 (0.10)	1156 (sh)	1069 (0.36)	1067 (0.41)	1065 (1.26)
1150 (0.46)	925 (0.24)	1071 (0.63)	987 (0.20)	1068 (1.65)	813 (0.18)	1082 (0.11)	960 (0.14)	996 (0.09)	1019 (sh)
1068 (1.00)	878 (sh)	985 (0.20)	865 (0.19)	996 (0.81)	760 (sh)	989 (0.63)	839 (0.16)	868 (sh)	908 (0.09)
972 (0.15)	809 (0.47)	882 (0.43)	766 (sh)	880 (sh)	691 (0.12)	881 (0.25)	736 (0.13)	740 (0.18)	812 (0.28)
878 (sh)	753 (sh)	755 (0.22)	646 (0.27)	825 (0.68)	581 (sh)	769 (0.48)	614 (0.10)	649 (0.14)	741 (1.41)
814 (0.38)	587 (0.44)	556 (0.51)	479 (sh)	695 (0.32)	525 (sh)	611 (0.63)	477 (0.34)	465 (0.14)	670 (0.73)
758 (sh)	467 (0.7)	468 (0.34)	443 (sh)	604 (1.02)	474 (0.14)	595 (sh)	434 (0.10)	446 (sh)	633 (sh)
681 (0.38)	439 (0.79)	449 (0.44)	423 (2.13)	492 (sh)	459 (sh)	583 (0.16)	411 (0.24)	410 (0.23)	603 (sh)
544 (0.33)	423 (0.81)	414 (2.06)		472 (0.81)	423 (0.15)	561 (sh)			462 (0.98)
464 (0.89)	409 (0.90)			443 (sh)					442 (1.00)
433 (2.36)				423 (0.89)					414 (2.45)

[a] A (10 Torr CS_2; 36 mJ/cm^2); B (50 Torr CS_2; 20 mJ/cm^2); C (50 Torr CS_2; 44 mJ/cm^2); D (100 Torr CS_2; 36 mJ/cm^2); E (50 Torr CS_2; 52 mJ/cm^2); F (50 Torr CS_2; 76 mJ/cm^2); G (100 Torr CS_2; 36 mJ/cm^2, in excess of nitrogen).

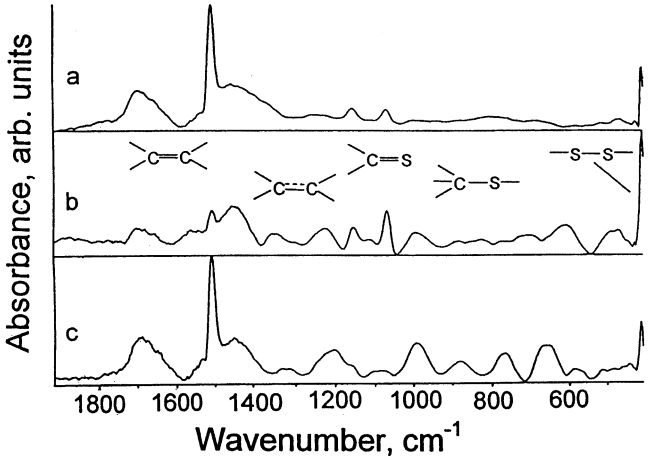

Figure 1. FTIR spectra of dark brown (a), light brown (b), and golden (c) deposited solid from UV photolysis of CS_2. (The band at 1508 cm^{-1}corresponds to adsorbed CS_2.)

insoluble and therefore highly cross-linked $(CS)_n$ polymer and elemental sulfur. The efficient removal of the elemental S by solvent implies that S (although incorporated) is not bonded to the polymer network.

We note that S removal by solvent was not attained with the $(CS_2)_n$ polymer obtained[15] by the long-wavelength photolysis of CS_2. The analyses presented below relate to deposited films that were not treated with the solvent.

FTIR Spectra. FTIR spectra of the sedimentary materials show rather broad absorption bands of medium to low absorbance, which indicates overlapping contributions of several vibrational modes. The very strong and sharp peak at 1508 (±2) cm^{-1} in all spectra, which disappeared completely after storing the materials under room temperature for several days, is attributed[20] to adsorbed CS_2. The comparison of the infrared spectra of these materials obtained under different irradiation condition (Table 1, Figure 1) reveals that they possess rather similar patterns of bands but differ somewhat from one another, mainly in the presence/absence of some bands and in their relative absorbance. The following band assignment is based on the knowledge of the IR spectra of model compounds.

The broad absorptions centered at 1684 (±10) cm^{-1} may be assigned[39] to ν(C═C) double bond stretches in conjugated carbonaceous systems experiencing strain in a ring.

The band centered at 1368−1446 cm^{-1} relates to C═C stretches shifted to lower wavenumbers due to multiple S substitution.[20] Thus, the band at 1446 (±5) cm^{-1} corresponds to the ν(C═C) double bond attached to four S atoms (e.g., 4,5-bis{[2-(methylthio)ethyl]thio}-1,3-dithiole-2-thione, 1453 cm^{-1}, ref 40; 4,4′,5,5′-tetrakis(decylthio)tetrathiofulvalene, 1461 cm^{-1}, ref 41) and its shoulders at 1403 and 1368 cm^{-1} are observed in similar four-sulfur-substituted >C═C< systems (e.g., 4,5-dimercapto-1,2-dithiole-3-thione,1400 cm^{-1}, ref 20; 4,5-bis-(methylthio)-1,3-dithiole-2-thione, 1418 cm^{-1}, ref 42; 4,5-bis(ethylthio)-1,3-dithiole-2-thione, 1368 cm^{-1}, ref 43). We note, however, that that region is also characteristic for ring vibrations of S heterocycles (1,3-dithiole-2-thiones,[40−43] tetrathiapentalenes[44]) and that the $\nu(S_2C{=}CS_2)$ stretches are overlapped with these modes.

The bands between 1200 and 1300 cm^{-1} are assigned[39] to skeletal stretches of C═C bonds.

The strong absorptions at 1155 (±5) and 1070 (±5) cm^{-1} are positioned in the region of the symmetric C═S stretch. The former band is characteristic[39] of ν(C═S) in dithiocarboxylates (−C−(C═S)−S−). These structures manifest themselves also at 580 and 900 cm^{-1} (as symmetric and asymmetric C−C═S stretches, respectively). The latter band is due to[39] ν(C═S) in trithiocarbonates −S−(C═S)−S− (also refs 20 and 45) that also displays itself through its asymmetric S−C═S stretches at ∼880 and 830 cm^{-1} and the symmetric stretch at ∼500 cm^{-1}. Although the assignment of the observed bands in the region of the ν(C═S) vibration is hampered by vibrational coupling of several different modes (C═S bending, C═C torsion, C−S stretch, ring modes), such assignment gets support from the ν(C═S) bands typical for the di- and trithiocarbonates.

The presence of very broad absorptions, with shoulders, centered at 473 (±5), 462 (±3), and 425 (±5) cm^{-1} is linked[20,39] with the S−S stretching mode. The absorptions at ∼570 and 470−480 cm^{-1} are characteristic of the ν(S−S) modes in aliphatic and aromatic disulfides, respectively. This suggests that the above-deduced C_nS_m structures are interconnected with disulfide bridges. This region is, however, also characteristic

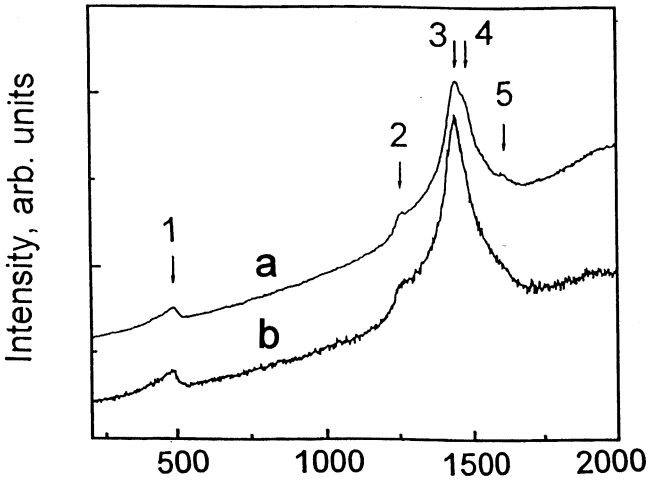

Figure 2. Raman spectrum of the solid deposited with long (a) and short (b) signal accumulation. The designated bands 1−5 are located, in the given order, at 480−495, 1255−1270, 1440−1449, 1475−1485, and 1610 cm^{-1}.

for sulfur allotropes that have their characteristic vibrations at 411 and 471 cm^{-1} (S_8, ref 46) and 402 and 476 cm^{-1} (S_7, ref 47). It is therefore conceivable that this low-wavenumber region is also contributed by the bands of the sulfur forms.

The difference in absorptivity of the characteristic bands of the materials (Table 1) deposited under different irradiation conditions (CS_2 pressure, incident energy, N_2 atmosphere) reflects different contents of various structures.

The effect of the incident irradiation fluence is seen from comparing the spectra of the deposits B, C, E, and F: an increase of the incident fluence at constant CS_2 pressure results in a decrease of the content of the trithiocarbonate moiety (ν(C═S) mode).

An increase in the CS_2 pressure leads to the pronounced deposition of the films with differently colored regions. The upward deposited films were always of golden color and the downward deposited layers contained always more dark brown and fewer light brown solids. The effect of the CS_2 pressure is given by the comparison of the spectra of the deposits A, C, and D. The dark brown material has the simplest spectra (deposits C and D), showing mainly the C═C, S_2C═CS_2, −C−(C═S)−S−, and −S−(C═S)−S− configurations, whereas the light brown and golden solids show additional absorptions in the region of weak[20] C═S vibrations (600−1000 cm^{-1}).

In N_2 atmosphere, the deposit has uniform (light brown) color and its spectral pattern includes, similarly to the golden material, absorption bands related to −C−S− vibrations. These bands are, however, positioned at different wavenumbers than for the golden film. The specific feature of this spectrum is a relatively high content of the >C═C< arrangements.

We suggest that (a) the light brown solid is a product of polymerization in the presence of deactivating collisions, (with N_2 or CS_2), (b) the dark brown solid is produced in the absence of these collisions, and (c) the golden solid forms from a hot (vibrationally excited) species moving upward in a heat convection current.

Raman Spectra. The Raman spectral data of all deposited materials (Figure 2) show similar spectral pattern, as observed for solid produced[10] by irradiation of CS_2 with a N_2 laser, and display the following frequences (intensities): 480−495 cm^{-1} (weak); 1255−1270 cm^{-1} (very weak); 1440−1449 cm^{-1} (strong); 1475−1485 cm^{-1} (shoulder); 1610 cm^{-1} (very weak); 2900 cm^{-1} (very weak). The band at 2900 cm^{-1} corresponds to two-photon-excited scattering.

TABLE 2: S $2p_{3/2}$ and C 1s Core Level Binding Energies and Populations, *P*, of Individual Sulfur and Carbon States

atom environment	BE (eV)	*P* (%) sample C[a]	*P* (%) sample D[a]	assignment
$S^{(1)}$	162.6	2.5	8.8	sulfide
$S^{(2)}$	163.5	17.6	26.1	S═C< (CS_2)
$S^{(3)}$	164.2	34.2	22.3	C−S, C−S−S−C, S^0
$S^{(4)}$	165.5	45.7	42.7	−S−O−
$C^{(1)}$	284.8	23.0	24.5	C−C
$C^{(2)}$	285.8	41.0	24.5	−C−S−
$C^{(3)}$	286.9	36.0	51.0	CS_2

[a] C (50 Torr CS_2; 44 mJ/cm^2); D (100 Torr CS_2; 36 mJ/cm^2).

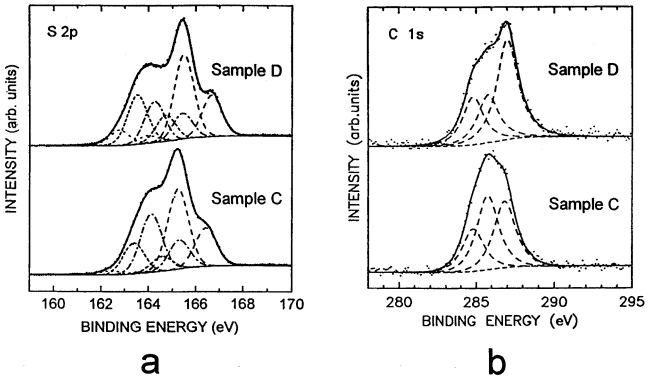

Figure 3. Fitted high-resolution spectra of S 2p (a) and C 1s (b) electrons in deposited solids.

The strongest band in all of the spectra is that centered at 1445 (±4) cm^{-1} with a shoulder at 1480 (±5) cm^{-1}. This band assigns[48] to the C═C stretch in (S_2)C═C(S_2) configuration, wherein S substitution shifts the ν(C═C) stretch to lower wavenumbers. The weak band at 1255−1270 cm^{-1} corresponds[49] to the ν(C═S) mode, whereas the band at 1610 cm^{-1} is likely due to a S═O stretch and reflects oxidation of some S centers with atmospheric oxygen. The spectra do not show any signal of a −C−S− stretch that is normally observed between 600 and 900 cm^{-1}. The band at 487 (±8) cm^{-1} is attributable[48] to a symmetric stretching motion of the C−S bond in the −S−(C═C)−S− configuration, but the absence of the asymmetric stretch at ca. 820 cm^{-1} (ref 50) makes this assignment improbable. It is therefore plausible to conclude that this band assigns to −S−S− bridges in polymeric −CS_2C− moieties (the typical S−S sym stretch at 510 cm^{-1}, refs 51 and 52), to the γ-deformation mode of S═C(S−)$_2$ unit in a trithiocarbonate configuration (at ca. 490 cm^{-1}),[53] and/or to sulfur allotropes S_6 and S_8 (at ∼470 cm^{-1}, refs 54 and 55).

The spectra moderately change upon longer exposition of the films to the excitation beam. The appearance of a new weak band at 1541 cm^{-1} and a bifurcation of the band at 1440−1449 cm^{-1} (Figure 2a) is in line with heat-induced structural changes in (S_2)C═C(S_2) configurations.

X-ray Photoelectron Spectra. XPS analyses were obtained for all the deposited materials (A−E), but reproducible results were only obtained for the solids C and D (Table 2). The data irreproducibility apparently resulted from thinness and inhomogeneity of the samples leading to different static charging of different deposit phases. The surface composition, $S_{1.0}C_{0.32}O_{0.13}$ (sample C) and $S_{1.0}C_{0.41}O_{0.042}$ (sample D), reveals somewhat more than 2-fold excess of sulfur over carbon and indicates slight oxidation of the superficial layers.

The S 2p core level spectrum (Figure 3a) is best fitted with contributions of four different chemical states of S (each represented by the spin−orbit doublets with separation Δ($2p_{3/2}$,

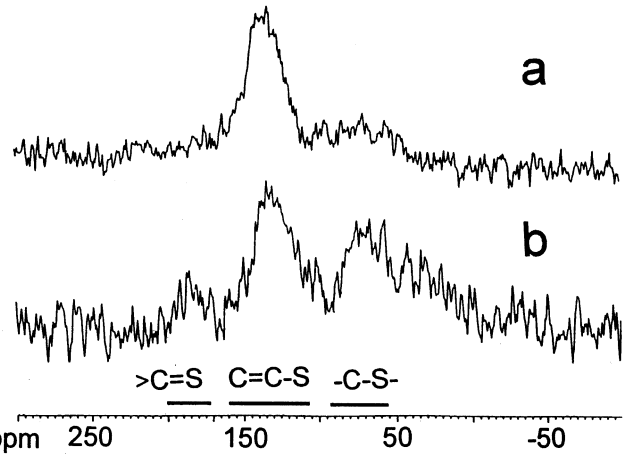

Figure 4. ^{13}C NMR MAS spectra of the deposited solids obtained in the absence (a, sample D) and presence of N_2 (b, sample G).

$2p_{1/2}$) = 1.18 eV and the intensity ratio $I(2p_{3/2})/I(2p_{1/2}) = 2/1$). The binding energies (BE, in eV) and the population (*P*, in % of total amount of S present) of these states for samples C and D are given in Table 2. The S $2p_{3/2}$ BE in order of increasing values can be interpreted[56,57,59] as contributions of sulfide S^{2-} (due to interaction of S with the Cu metal substrate), CS_2-like compounds (CS_2, 163.6 eV), elemental S (164.1 eV), and/or disulfide bridges ($(CH_3S)_2$ 164.3 eV, $(n\text{-}C_4H_9S)_2$ 164.1 eV, $(PhS)_2$ 164.4 eV) (or thiophene-like compounds (thiophene 164.3 eV)) and a structure in which S is bonded to O.

The C 1s core level spectrum (Figure 3b) shows three different chemical states of carbon that could be assigned[58] to (Table 2) to carbon in C−C, C−H bonds, C(−S) structures (285.5−287.5 eV), and C═S structures (CS_2, 287.0 eV).[59]

The XPS data are thus in line with the presence of elemental sulfur and of a C/S polymer containing both C−S and C═S bonds. They also indicate that the polymer incorporates more C═S bonds and fewer C−S bonds when the photolysis is carried out at higher CS_2 pressure and lower fluence.

^{13}C NMR Spectra. The ^{13}C NMR (MAS) spectra of the solid deposited in the absence and presence of N_2 (samples D and G, Figure 4) show a (major) broad peak at ∼110−160 ppm and a (minor) broad peak at ∼60−90 ppm that are assigned[42,60,61] to C═C in a heteroaromatic system (or to a >C═C−S− structure) and to a C−S− structure, respectively. A small broad peak at ∼175−200 ppm, due to the >C═S arrangement, is also apparent in sample D but not in G.

The difference points to a more feasible formation of polymeric C═S bonds in the presence of N_2. The broad signals are consistent with different environments of the distinguished structures that are likely due to cross-linked polymer network.

EPR Spectra. Disregarding the conditions of formation, the solid materials show a single line (Figure 5) with axial anisotropy, line width of 0.76 mT, and *g*-factor equal to 2.0044. Good agreement between the experimental and simulated EPR spectra was achieved using $g_\perp = 2.00429$, $g_{||} = 2.0107$, line width 0.69 mT, and Gauss/Lorentz ratio = 0.5.

The observed type of the EPR line with unresolved hyperfine structure is typical[20] for unpaired spin located on a sulfur orbital. The total concentration of unpaired spins amounted to 6.7×10^{18} per gram (the ratio of these unpaired spins to "CS_2" material 1:1180) and was not changed in the presence of air at room temperature. These findings indicate that the solid cross-linked deposits contain residual $-S\cdot$ radical centers; an examination of the paramagnetic behavior in the temperature range 0−200 °C reveals that the temperature dependence fulfills the Curie law and leads to no change in the concentration and the shape of the EPR signal.

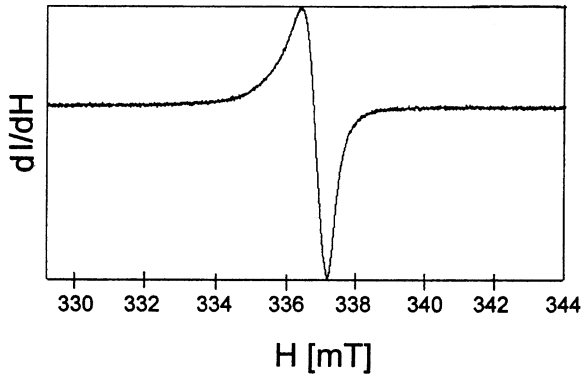

Figure 5. Typical EPR spectrum of the deposited solid.

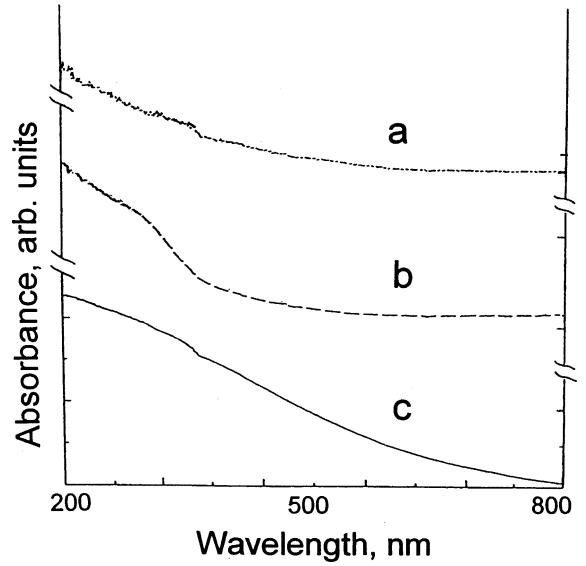

Figure 6. UV spectrum of the dark brown (a), light brown (b), and golden (c) solid.

The analyses thus indicate that the solids contain S-centered radicals that are stable in air and withstand heating in a H_2 atmosphere.

UV Spectra. UV spectra of the dark brown, light brown, and golden materials show absorption descending from 200 nm to higher wavelengths (Figure 6). More pronounced absorption between 350 and 600 nm for the golden polymer is compatible with a relatively higher degree of conjugation in this polymer.

Electron Microscopy Analysis. Morphology of the solids deposited in the CS_2 photolysis in the absence of nitrogen using different fluences and in the excess of nitrogen reveals some different features.

The SEM images of the solid films from the photolysis of CS_2 in the absence of N_2 (sample D) show nonuniformly (100−300 nm) sized spherical bodies that bond together by either coalescing into smooth bodies (Figure 7a) or forming fluffy structures (Figure 7b). The SEM images of the solid films obtained under excess of nitrogen (sample G) indicate similar round shape bodies (Figure 7c) that form fluffy structures (Figure 7d).

TEM images of the solids samples (Figure 8) reveal that the particles obtained in the excess (sample G) and absence of N_2 (sample D) have very different features. The former particles are compact solid spheres with a size greater than 50 nm, whereas the latter consist of ca. 20−40 nm thick ca. 100−200 nm sized hollow spheres.

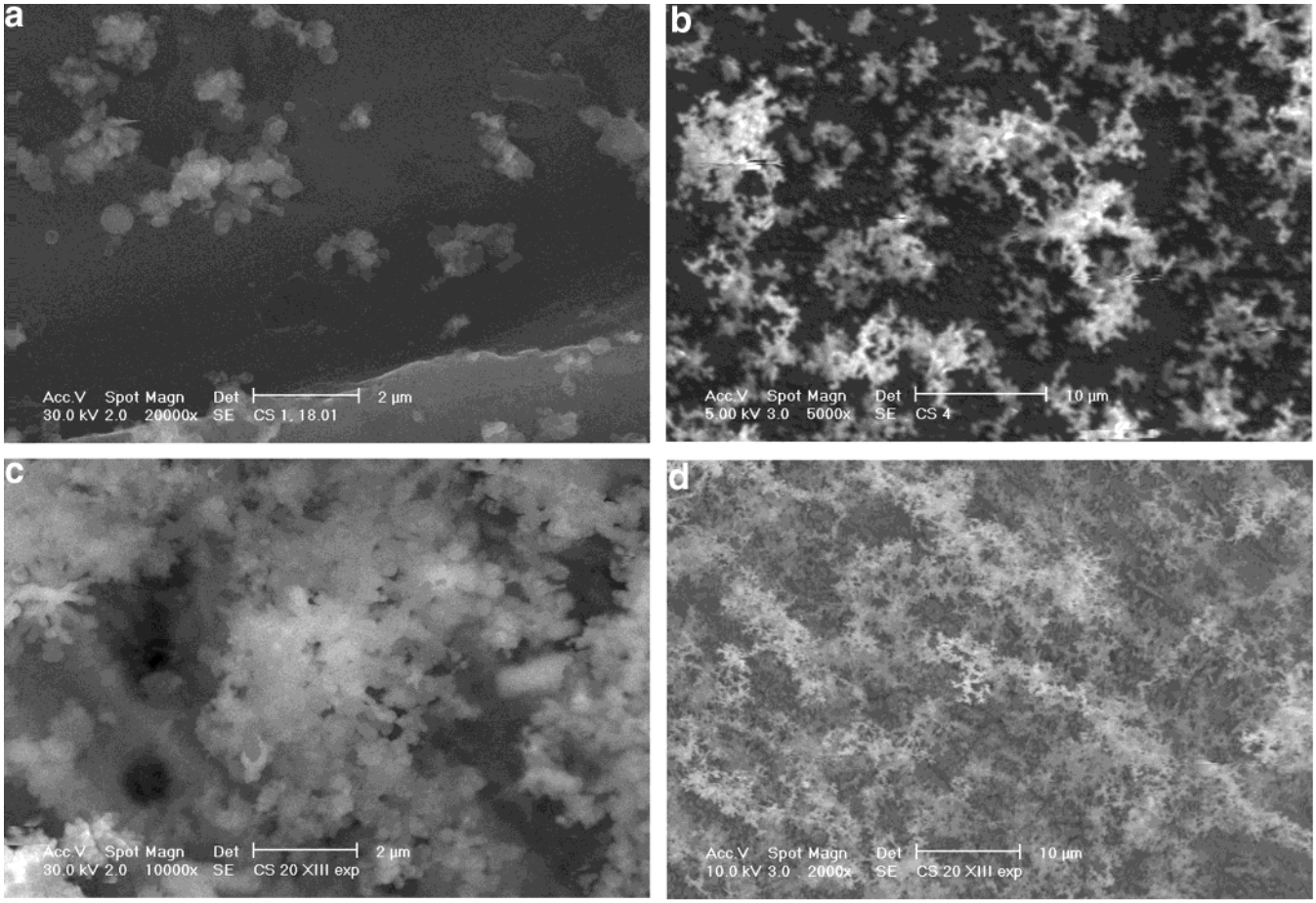

Figure 7. SEM images of the solids deposited in the absence (a, b) and excess (c, d) of N_2.

The hollow spheres are interesting nanosized features that were not observed[11,15,20] in the long-wavelength photolytic polymerization of CS_2.

Thermal Stability.

TGA Analysis. Thermograms of the solid deposits are commonly two-stage processes showing a sharp decrease of the weight to ca. 50% between ca. 180 and 220 °C and a further slower decrease of the weight to no residue between 300 and 800 °C. This heating in Ar leads to an evaporation of a solid material whose FTIR spectrum (1430 cm^{-1} (vs), 1023 cm^{-1} (m), 880 cm^{-1} (m) 800, 714, 540, 470, and 412 cm^{-1} (all w)) is consistent with a C/S polymer possibly containing sulfur allotropes.

This thermal behavior is completely different from that of the $(CS_2)_n$ polymer obtained from the long-wavelength CS_2 photolysis, which undergoes[15] only 4% weight loss at 200 °C and degrades more significantly (ca. 25% weight loss) only at ca. 320 °C.

Mass-Spectral Analysis. Heating the samples under high vacuum of the direct inlet of the mass spectrometer) reveals the occurrence of signals (*m*/*z* 64, 96, 128, 160, 192, 224, and 256). These signals are observed at 180−200 °C and they confirm the presence of S_{2-8} species. (We note that the identical MS spectrum is observed with elemental sulfur.) The weight loss due to the extrusion of the S species corresponds to ca. 50% of the initial sample and leads to a black residue decomposing at 300 °C.

The weight depletion corresponding to slightly more than the S_n portion in (C_nS_{2n}) indicates that evaporation of the incorporated elemental sulfur is accompanied by an additional but minor process consisting of extrusion of sulfur liberated through thermal reorganization (S—S cleavage) of the polymer structure.

This observation indicates that the decomposition pattern is completely different from that of the $(CS_2)_n$ polymer[15] that shows minor peaks of CS, CS_2, and S_2 at 155 °C and predominant peaks of CS and S_2 near 200 °C.

FTIR Spectral Analysis. Heating the samples to 80 ° C for 2 h in Ar results in significant changes in relative absorbance of some IR spectral bands (Figure 9) and reveals that structural reorganizations in the solids can be induced even at such low temperature. The spectral changes in the solids obtained in both the absence and excess of N_2 reflect an increase in the >C═C< structures unattached to S (the band at ∼1680 cm^{-1}) and the decrease of the $S_2C{=}CS_2$ structures (the broad band at ∼1370−1500 cm^{-1}). Apart from that, the solids obtained in the absence of N_2 experience spectral changes in the ν(C═S) region and those obtained in the excess of N_2 are modified in the region of −C−S− structures (below 1000 cm^{-1}).

The upper and lower curves relate to the initial and heated films, respectively.

The FTIR spectral observations indicate that structural changes observed at ca. 200 °C are preceded with low-temperature (80 °C) structural reorganizations, allowing at higher temperatures in Ar the extrusion of a polymer (or polymerizing) fraction and in high vacuum the elimination of elemental sulfur.

The observed extrusion of polymeric fractions and sulfur beginning at below 200 °C indicates scission of S—S bonds (known to take place in disulfides below 150 °C and have a complex character) and disproves the possibility of the C−S

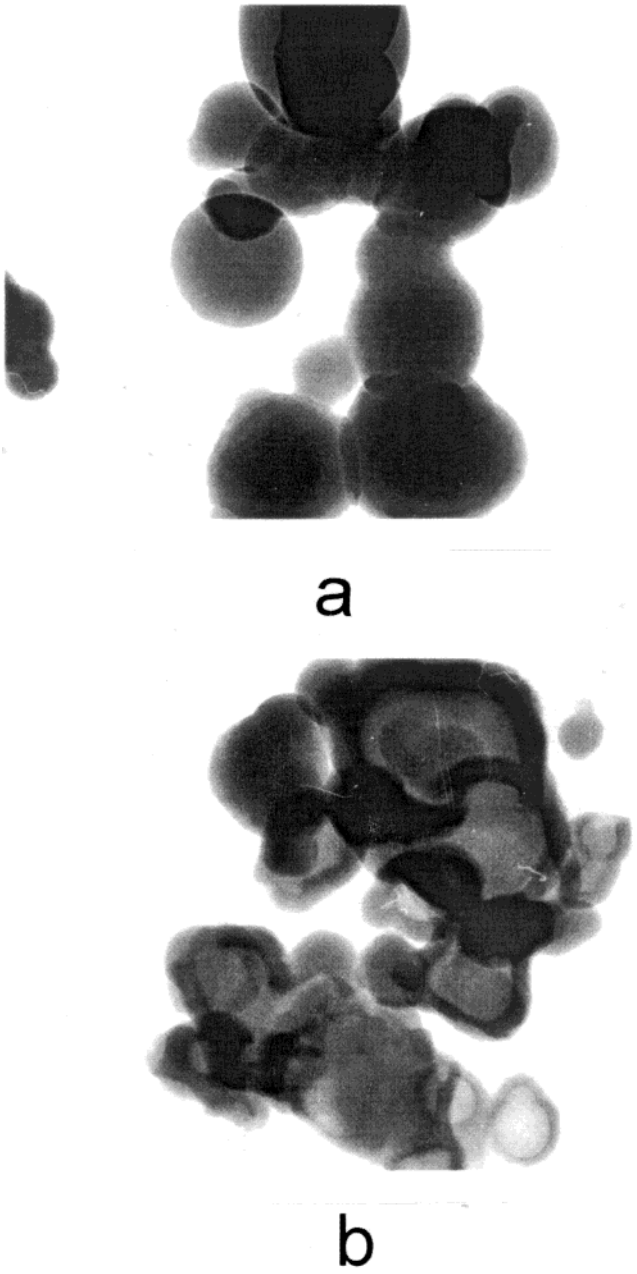

Figure 8. TEM images of the solids deposited in the excess (a) and absence (b) of N_2.

splits (that normally occur at temperatures at least by three hundred degrees higher).[62]

3.2. Photolytic Features and Probable Mechanism of Solid Formation. UV photolysis of carbon disulfide via excitation in its absorption system between 185 and 230 nm is known[63,64] to result in predissociation to CS fragments and sulfur atoms. The process induced with intense ArF laser radiation[22,23,25,27,65] proceeds via a single- and double-photon excitation and results in the formation of energy-rich (excited) CS fragments and S atoms in ^{3}P and ^{1}D states. In our conditions of high CS_2 pressure, the photolytic process is controlled by a two-photon excitation. This turns out from the laser-fluence-dependent depletion of CS_2, which shows (Figure 10) the slope for a double-logarithmic plot close to 2.

According to the literature data,[21,64] both direct and/or sequential two photon excitation (Scheme 1) is energetically feasible and yields S (^{1}D) and S (^{3}P). These atoms were detected in this work through scavenging experiments with ethene. The

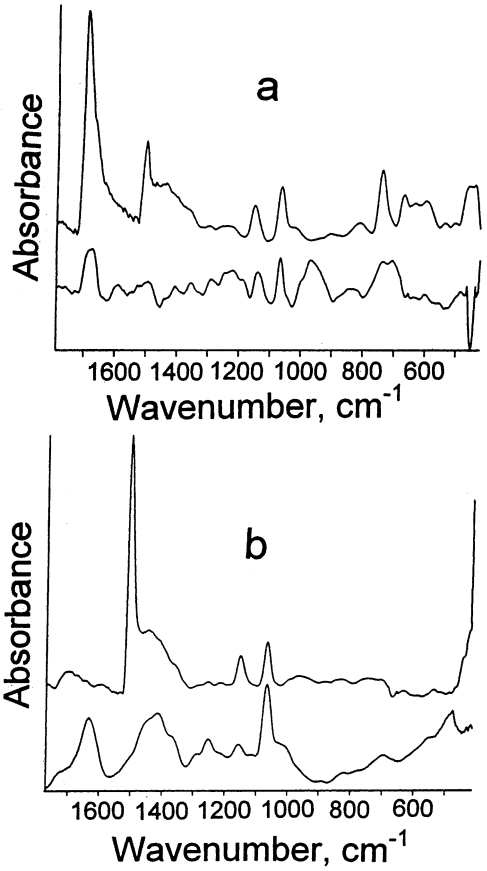

Figure 9. FTIR spectra of deposits obtained in the excess (a) and the absence (b) of N_2 heated to 80 °C.

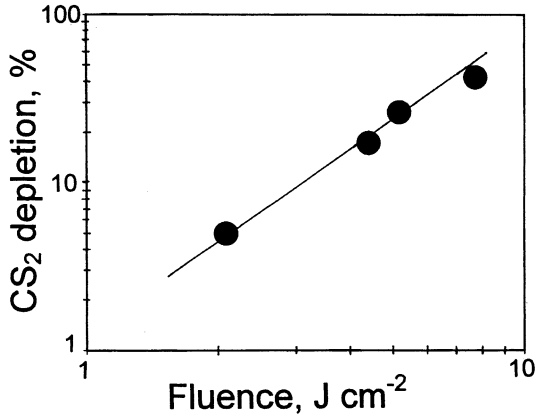

Figure 10. Depletion of CS_2 (10 min irradiation, 50 Torr) as a function of incident laser fluence.

SCHEME 1

$$CS_2 + h\upsilon \rightarrow CS_2^*$$

$$CS_2^* + h\upsilon \rightarrow CS^* + S\ (^1D)$$

$$CS^* \rightarrow C(^3P) + S\ (^3P)$$

$$CS^* + CS_2 \rightarrow CS + CS_2^*$$

$$CS_2^* \rightarrow CS + S\ (^3P)$$

$$\rightarrow CS + S\ (^1D)$$

ArF laser photolysis of CS_2 (in the absence and excess of N_2) in the presence of admixture of ethene yielded, apart from a brown depositing solid, mixtures of thiirane (TH) and ethenethiol

SCHEME 2

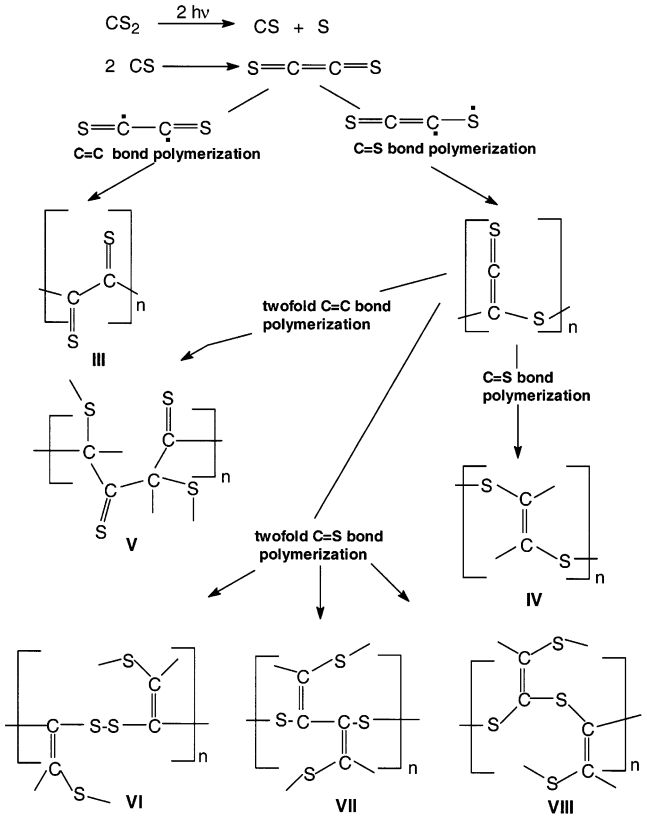

(ET) as major and hydrogen sulfide and thiophene as minor volatile products. It is regarded[66] that ET arises exclusively from the reaction of S (^{1}D) with ethene, and that TH is formed via reaction of S (^{1}D) or S (^{3}P) with ethene. In these reactions,[67,68] TH forms solely via addition (and stabilization) of the adduct, whereas ET is produced via direct insertion into the C−H bond and by rearrangement of hot TH. In all of our experiments, the ratio of the TIC (total ion current) MS signals for ET and TH (ET/TH) was ∼1:3. The constancy of the value reveals poor collisional efficiency of N_2 to quench S (^{1}D) atoms and implies that the observed differences in spectral properties of the solid products obtained in the absence and excess of N_2 are not caused by different proportions of S (^{1}D) and S (^{3}P) atoms.

We suggest that the formation of the highly cross-linked $(CS)_n$ polymer, containing the assessed >C═S, >C═C<, S_2C═CS_2, −C−(C═S)−S−, −S−(C═S)−S−, and C−S−S−C configurations, takes place via a dimerization of the CS fragment into ethylenedithione[69−72] (known as extremely unstable at partial pressures above 10^{-4} mbar[72]) that undergoes polymerization at both C and S centers (Scheme 2).

The formation of C_2S_2 is regarded as a combination[71] of singlet and triplet CS species, which gets support from a theoretical prediction[73] that the collinear reaction of ground-state CS to C_2S_2 requires UV excitation. The occurrence of both singlet and triplet CS states is conceivably due to a considerable excess of energy delivered to CS_2 molecules upon absorption of two photons ($h\nu$ at 193 nm = 620 kJ/Einstein, C═S bond dissociation energy ∼440 kJ/mol[12]) and the population of several high-energy CS states during ArF photolysis.[22,25,27,65] We admit, however, that this simple scheme is likely contributed by reactions of CS or C_2S_2 with oligomeric products.

The structures III−VIII contain all the observed configurations except for trithiocarbonate. We conclude that the −S−(C═S)−S− arrangement is either produced via (a) a sequence of two reactions between two CS fragments (via 2-fold nucleophilic attack of S center on C) or via (b) a 1,3-S→C rearrangement in structure VI. The ground-state CS (theoretically described[74] as $C^{\delta+}$—$S^{\delta-}$) behaves as a weak Lewis acid,[75] C-centered electrophile,[76] inserts into some polar bonds,[77] and is similar to electron-rich carbenes.[77] Differentiation between path a and b is, however, difficult, because reactivity modes of the excited species are unknown. We assume that the rearrangement mode gets some support from the aforementioned structural modification of the solid deposits taking place upon mild heating.

The above rationale reveals that the mechanism of the polymer formation cannot be depicted by an important intermediate creating the main unit of the polymer structure. As stressed by the observation of different (dark brown, light brown, and golden) polymeric materials, the polymer formation is quite complex and the path contributing to its formation varies with experimental conditions but also in different regions of the irradiated gas volume.

4. Conclusions

ArF laser photolysis of gaseous CS_2 results in chemical vapor deposition of elemental sulfur and nanostructured $(CS)_n$ polymer whose formation is interpreted in terms of CS polymerization in the gas phase.

The gas-phase polymerization of CS differs from the CS decay through a heterogeneous wall reaction[30] in the absence of a UV excitation source.

The polymer is composed of nonadherent dark brown and light brown films and tenaciously adherent golden films; their relative extent is affected by the irradiation conditions and reactor region.

The proposed polymerization mechanism of CS is explained by an intermediacy of C_2S_2 species.

The depletion of CS_2 is controlled by two-photon absorption. Scavenging experiments with ethene revealed the constant ratio of thiirane and ethenethiol (major products) under all irradiating conditions and confirmed that different properties of the polymeric $(CS)_n$ polymer are not due to different extents of S (^{1}D) and S (^{3}P) atoms.

The $(CS)_n$ polymer contains S-centered radicals that are stable in air and withstand heating in H_2 atmosphere. Its structure is contributed by >C═S, >C═C<, S_2C═CS_2, −C−(C═S)−S−, −S−(C═S)−S− and C═S−S−C configurations whose relative extent depends on irradiation conditions: more C═S bonds (and fewer C−S bonds) are formed at higher CS_2 pressure, in the excess of N_2 and with lower laser fluences.

The sensitivity of the polymer toward mild heating is in line with a decrease in S_2C═CS_2 units (and an increase in >C═C< units).

The polymer deposited in the absence of N_2 consists of unique 100−200 nm sized hollow spheres that are appealing for nanoapplications.

Acknowledgment. We thank Dr. A. Galíková and Dr. A. Galik for TGA analysis and Dr. V. Blechta for NMR measurements. Support by the Ministry of Education, Youth and Sports (Grant ME 484) and by the Academy of Sciences of the Czech Republic (Grant no. AVOZ1-010-914) is gratefully acknowledged.

References and Notes

(1) Loew, O. *Z. Chem.* **1868**, *4*, 622.
(2) Sidot, M. T. C. *R. Hebd. Seances Acad. Sci.* **1872**, *74*, 179.

(3) Rabalais, J. W.; McDonald, J. M.; Sherr, V.; McGlynn, S. P. *Chem. Rev*. **1971**, *71*, 73.
(4) de Sorgo, M.; Yarwood, A. J.; Strausz, O. P.; Gunning, H. E. *Can. J. Chem*. **1965**, *43*, 1886.
(5) Ernst, K.; Hoffman, J. J. *Chem. Phys. Lett*. **1979**, *68*, 40.
(6) Ernst, K.; Hoffman, J. J. *Chem. Phys. Lett*. **1980**, *75*, 388.
(7) Wen, F. C.; McLaughlin T.; Katz, J. *Phys. Rev*. **1982**, *26*, 2235.
(8) Chen, C.-C.; Katz, J. L. *J. Phys. Chem*. **1987**, *91*, 2504.
(9) Y. P. Vlahoyannis, Y. P.; Patsilinakou E.; Fotakis, C.; Stockale, J. A. D. *Radiat. Phys. Chem*. **1990**, *36*, 523.
(10) Matsuzaki, A.; Hamada, Y.; Morita, H.; Matsuzaki, T. *Chem. Phys. Lett*. **1992**, *190*, 337.
(11) Matsuzaki, A.; Morita, H.; Hamada, Y. *Chem. Phys. Lett*. **1992**, *190*, 331.
(12) Safarik, I.; Strausz, O. P. *Res. Chem. Intermed*. **1991**, *16*, 225.
(13) Gingell, J. M.; Mason, N. J.; Sutherland, J.; Taylor, M. *Meas. Sci. Technol*. **1994**, *5*, 1281.
(14) Cataldo, F. *Inorg. Chim. Acta* **1995**, *232*, 27.
(15) Colman, J. J.; Trogler, W. C. *J. Am. Chem. Soc*. **1995**, *117*, 11270.
(16) Colman, J. J.; Xu, X.; Thiemens, M. H.; Trogler, W. C. *Science* **1996**, *273*, 774.
(17) Makarov, V. I.; Khmelinskii, I. V. *J. Photochem. Photobiol. A: Chem*. **1998**, *119*, 147.
(18) Zmolek, P. B.; Xu, X.; Jackson, T.; Thiemens, M. H.; Trogler, W. *J. Phys. Chem*. **1999**, *103*, 2477.
(19) Heymann, D.; Cataldo, F.; Thiemens, M. H.; Fokkens, R.; Nobbering, N. M. M.; Vis, R. D. *Meteor. Planet. Sci*. **2000**, *35*, 355.
(20) Zmolek, P. B.; Sohn, H.; Gantzel, P. K.; Trogler, W. C. *J. Am. Chem. Soc*. **2001**, *123*, 1199.
(21) Loree, T. R.; Clark, J. H.; Butterfield K. B.; Lyman J. L.; Engleman R. *J. Photochem*. **1979**, *10*, 359.
(22) Butler, J. E.; Drozdoski, W. S.; McDonald, J. R. *J. Chem. Phys*. **1980**, *50*, 413.
(23) Yang, S. C.; Freedman, A.; Kawasaki, M.; Bersohn, R. *J. Chem. Phys*. **1980**, *72*, 4058.
(24) Addison, M. C.; Donovan, R. J.; Fotakis, C. *Chem. Phys. Lett*. **1980**, *74*, 58.
(25) McCrary, V. R.; Lu, R.; Zakheim, D.; Russell, J. A.; Halpern, J. B.; Jackson, W. M. *J. Chem. Phys*. **1985**, *83*, 3481.
(26) Desai S. R.; Feigerle, F. C.; Miller J. C. *J. Phys. Chem*. **1995**, *99*, 1786.
(27) Kitsopoulos, T. N.; Gebhardt, C. R.; Ratzikis, T. P. *J. Chem. Phys*. **2001**, *115*, 9727.
(28) Bridgman, P. W. *J. Appl. Phys*. **1941**, *12*, 466.
(29) Wood, W. P.; Heicklen, J. *J. Phys. Chem*. **1971**, *75*, 854.
(30) Richardson, R. J.; Powell, H. T.; Kelley, J. D. *J. Phys. Chem*. **1973**, *77*, 2601.
(31) Farges J. P. *Organic Conductors*; M. Dekker, New York, 1994.
(32) Crayston, J. A.; Iraqi A.; Walton, J. C. *Chem. Soc. Rev*. **1994**, *23*, 147.
(33) Bredas, J. L.; Silbey, R. In *Conjugated Polymers*; Bredas, J. L., Silbey, R., Eds.; Kluwer Academic: Dordrecht, The Netherlands, 1991.
(34) Genin, H.; Hoffmann, R. *J. Am. Chem. Soc*. **1995**, *117*, 12328.
(35) Pola, J.; Lycka, A.; Gusel'nikov, L. E.; Volkova, V. V. *J. Chem. Soc., Chem. Commun*. **1991**, 20.
(36) Pola, J.; Bastl, Z.; Šubrt, J.; Abeysinghe, J. R.; Taylor, R. J. *Mater. Chem*. **1996**, *6*, 155.
(37) Pola, J.; Urbanová, M.; Bastl, Z.; Šubrt, J.; Sakuragi, M.; Ouchi, A.; Morita, H. *Polymer* **2001**, *42*, 1311.
(38) Pola, J.; Galíková, A.; Galík, A.; Blechta, V.; Bastl, Z.; Šubrt, J.; Ouchi, A. *Chem. Mater*. **2002**, *14*, 144.
(39) *Infrared Structural Correlation Tables and Data Cards*; Miller, R. G. J., Willis, H. A., Eds.; Heyden & Son Ltd., Spectrum House: London, 1969; Tables 1 and 2.
(40) Hurley, M. F.; Chambers, J. Q. *J. Org. Chem*. **1981**, *46*, 775.
(41) Park, R. P.; Kilburn, J. D.; Ryan, T. G. *Synthesis* **1994**, 195.
(42) Hartke, K.; Hoppe, H. *Chem. Ber*. **1974**, *107*, 3121.
(43) Reuter, U.; Gatow, G. *Z. Anorg. Allg. Chem*. **1976**, *421*, 143.
(44) Kimura, S.; Kurai, H.; Mori, T.; Mori, H.; Tanaka, S. *Bull. Chem. Soc. Jpn*. **2001**, *74*, 59.
(45) Tamami, B.; Kiasat, A. R. *J. Chem. Res. (S)* **1998**, 454.
(46) Nimon, L. A.; Neff, V. D.; Cantley, R. E.; Buttlar, R. O. *J. Mol. Spectrosc*. **1967**, *22*, 105.
(47) Gardner, M.; Rogstad A. *J. Chem. Soc., Dalton* **1973**, 599.
(48) Dyer, C. D.; Kilburn, J. D.; Maddams, W. F.; Walker, P. A. *Spectrochim. Acta A* **1991**, *47*, 1225.
(49) Ozaki, Y.; Storer, A. C.; Carey, P. R. *Can. J. Chem*. **1982**, *60*, 190.
(50) Herzog, K.; Steger, E.; Rosmus, P.; Scheithauer, S.; Mayer, R. *J. Mol. Struct*. **1969**, *3*, 339.
(51) Williams, C. R.; Britten, F. J.; Harpp, D. N. *J. Org. Chem*. **1994**, *59*, 806 and references therein.
(52) Meyer, M. *J. Mol. Struct*. **1992**, *273*, 99.
(53) Herzog, K.; Fabian, J. *Z. Phys. Chem*. **1995**, *191*, 159.
(54) Nimon, L. A.; Neff, V. D.; Cantley, R. E.; Buttlar, R. O. *J. Mol. Spectrosc*. **1967**, *22*, 105.
(55) Scott, D. W.; McCullough, J. P. *J. Mol. Spectrosc*. **1964**, *13*, 313.
(56) *Practical Surface Analysis Vol 1 Auger and X-ray Photoelectron Spectroscopy*; Briggs, D., Seah, M. P., Eds.; John Wiley and Sons: Chichester, U.K., 1990; p 604.
(57) *NIST X-ray Photoelectron Spectroscopy Database* ver. 2.0; NIST Standard Reference data Program; NIST: Gaithersburg, MD, 1997.
(58) Briggs D.; Beamson G. *High-Resolution XPS of Organic Polymers, The Scienta ESCA300 Database*; John Wiley and Sons: Chichester, U.K., 1992.
(59) Gelius, U.; Heden, P. F.; Hedman, J.: Lindberg, B. J.; Manne, R.; Nordberg, R.; Nordling, C.; Siegbahn, K. *Phys. Scr*. **1970**, 2, 70.
(60) Levy, G. C.; Nelson, G. L. *Carbon-13 Nuclear Magnetic Resonance for Organic Chemists*; Wiley: New York, 1972.
(61) Turner, W. V.; Pirkle, W. H. *J. Org. Chem*. **1974**, *39*, 1935.
(62) Strausz, O. P.; Gunning, H. E.; Lown, J. W. In *Comprehensive Chemical Kinetics*; Bamford, C. H., Tipper, C. F. H., Eds.; Elsevier: Amsterdam, 1972; Vol. 5, Chapter 6.
(63) Douglas, A.; Zanon, J. *Can. J. Phys*. **1964**, *42*, 627.
(64) Rabalais, J. W.; McDonald, J. R.; Scherr, V.; McGlynn, S. P. *Chem. Rev*. **1971**, *71*, 73.
(65) Dornhofer, G.; Hack, W.; Langel, W. *J. Phys. Chem*. **1984**, *88*, 3060.
(66) Wiebe, H. A.; Knight, A. R.; Strausz, O. P.; Gunning, H. E. *J. Am. Chem. Soc*. **1965**, *87*, 1443.
(67) Sherwood, A. G.; Safarik, I.; Verkoczy, B.; Almadi, G.; Wiebe, H. A.; Strausz, O. P. *J. Am. Chem. Soc*. **1979**, *101*, 3000.
(68) McKee, M. L. *J. Am. Chem. Soc*. **1986**, *108*, 5059.
(69) Sülzle, D.; Schwarz, H. *Angew. Chem*. **1988**, *100*, 1384.
(70) Maier, G.; Reisenauer, H. P.; Schrot, J.; Janoschek, R. *Angew. Chem*. **1990**, *102*, 1475.
(71) Bohn, R. B.; Hannachi, Y.; Andrews, L. *J. Am. Chem. Soc*. **1992**, *114*, 6452.
(72) Wentrup, C.; Kambouris, P.; Evans, R. A.; Owen, D.; Macfarlane, G.; Chuche, J.; Pommelet, J. C.; Cheikh, A. B.; Plisnier, M.; Flammang, R. *J. Am. Chem. Soc*. **1991**, *113*, 3130.
(73) Gomez-Jeria, J. S.; Morales, R. G. E.; Reyes, L. M. *Astrophys. J*. **1986**, *302*, 488.
(74) Schnöckel, H.; Köppel, R. *J. Am. Chem. Soc*. **1989**, *111*, 4583.
(75) Klabunde, K. J.; White, C. M.; Efner, H. F. *Inorg. Chem*. **1974**, *13*, 1778.
(76) Moltzen, E. K.; Senning, A.; Lütjens, H.; Krebs, A. *J. Org. Chem*. **1991**, *56*, 1317.
(77) Moltzen, E. K.; Kramer, M. P.; Senning, A.; Klabunde, K. J. *J. Org. Chem*. **1987**, *52*, 1156 and references therein.